

# Spin-Exchange Collisions in Optical Pumping of $^{129}\text{Xe}$ : A Multiscale Simulation

Perttu Hilla,<sup>1</sup> Marko Tuomela,<sup>1</sup> Jyrki Rantaharju,<sup>1</sup> and Juha Vaara<sup>1</sup>

<sup>1</sup>*NMR Research Unit, P.O. Box 3000, FI-90014 University of Oulu, Finland\**

Xenon nuclei may be hyperpolarized through collisions with optically pumped rubidium, with the Xe hyperfine coupling (HFC) between the unpaired Rb electron and xenon nucleus transferring spin polarization from the Rb atom to Xe. We model the polarization transfer to  $^{129}\text{Xe}$  in short binary collisions and long van der Waals (VDW) complexes between gaseous Rb and Xe. The simulations feature molecular dynamics of the Rb-Xe mixture, spin-Hamiltonian parameters extracted from relativistic quantum chemistry, and explicit spin dynamics simulations of the Rb-Xe interaction events on a novel Python code. Oscillation in the VDW bond-length  $R$  strongly modulates the Xe HFC, imposing steps in the Xe polarization build-up. The Rb nucleus and the unpaired electron constitute a strongly coupled two-spin system, with practically constant Rb HFC regardless of  $R$ . Explicit numerical propagation of the time-dependent Schrödinger equation for a simplified model VDW complex reveals that the spin system undergoes two simultaneous Rabi-like oscillations between the initial, fully spin-polarized state of the Rb atom, and two final states after the Xe spin flip, one in each of the two branches of the hyperfine spectrum of the Rb atom. The simulations indicate that incorporating the Rb HFC explicitly results in an overall reduction of the Xe polarization as compared to the simple model, in which the Rb HFC is neglected. Slow oscillations between the Rb spin states constitute an envelope on which the steps in the Xe polarization are superimposed, and this determines the achievable Xe polarization in long-lived VDW events. A simple empirical polarization transfer model based on the lifetime distribution of the VDW events and the Rabi transition probabilities reveals that, in the simulated conditions, a large part of the polarization transfer takes place due to the transition between separate branches of the hyperfine states of the Rb atom. This is due to the fact that maxima of the transition probability can, for this faster oscillation, be reached within the lifetime of the VDW complexes. We expect that these findings will contribute to the understanding of the spin-exchange optical pumping process and aid in its optimization.

Keywords: noble gas, alkali metal, spin exchange, polarization transfer, nuclear magnetic resonance, hyperfine coupling

## I. INTRODUCTION

The sensitivity in nuclear magnetic resonance spectroscopy and magnetometry is affected by the degree of nuclear spin polarization, which is in normal experimental conditions rendered small by thermal fluctuations nearly equalizing the spin populations [1]. Spin-exchange optical pumping (SEOP) [2–4] is one of the hyperpolarization methods [5] that furnish nuclear spins polarized beyond thermal equilibrium. In SEOP, large polarization level of noble-gas nuclei, *e.g.*,  $^{129}\text{Xe}$ , can be obtained via interactions with alkali metal atoms in the gas phase, *e.g.*, Rb. In the process, the atomic states of Rb are polarized by continuous irradiation with circularly polarized light. The polarization transfer to the Xe nucleus occurs in gas-phase interaction events that range from short binary collisions [6–8] to long-lived van der Waals (VDW) complexes [6, 9–13] of the Rb-Xe pair. The key interaction in the transfer is the hyperfine coupling (HFC) between the unpaired electron of the Rb atom and the spin-1/2  $^{129}\text{Xe}$  nucleus.

The roles played by the other microscopic interactions in the polarization transfer have been studied theoretically and experimentally. They include the HFC to the  $^{85/87}\text{Rb}$  nucleus [14–16], which establishes the coupled

spin-state system of the Rb atom, the spin-rotation interactions of the unpaired electron [9, 11, 12, 15, 17–20] and of the  $^{129}\text{Xe}$  nucleus [21], thought to mainly affect relaxation of the electron and nuclear spins, respectively, paramagnetic interactions with the impurities in the polarization cell walls [22] (also causing xenon relaxation [21]), nuclear quadrupole coupling (NQC) interaction, and nuclear spin-spin interactions. In the NQC context, hyperpolarization of the quadrupolar  $^{131}\text{Xe}$  nucleus (spin 3/2) has been demonstrated [23].

While theoretical models of SEOP dynamics [6, 12, 13, 24] and macroscopic modeling of the physics within the polarization cell [25–31] have been presented, simulations have not yet been widely used to account for the microscopic details of the polarization transfer. Ref. 32 applied a coarse-grained, stochastic many-body method to investigate the coupled dynamics of the alkali atom and noble gas spins at the ensemble level, averaging over the molecular-level details. Ref. 16 applied *ab initio* calculations of the atomic interaction potentials and HFC, as well as scattering theory to define upper limits of the attainable  $^3\text{He}$  polarization, as well as the spin-exchange rates in SEOP with  $^{39}\text{K}$  and  $^{107}\text{Ag}$ . Overall, the modeling situation leaves potential for further computational optimization of the SEOP technique. To meet this demand, we have proposed a first-principles multiscale simulation approach for the polarization exchange events in gas-phase collisions between Rb and  $^{129}\text{Xe}$  [20].

---

\* juha.vaara@oulu.fi

The method combines detailed molecular dynamics (MD) simulation of atomic trajectories in the gas mixture, sampled by quantum-chemical (QC) calculations of the spin Hamiltonian parameters. These Hamiltonians are, in turn, used to drive spin dynamics (SD) of the combined density matrix of the spins  $\hat{S}$  and  $\hat{K}$  of the unpaired electron of Rb and the xenon nucleus, respectively. The method was in Ref. 20 applied to investigate the polarization transfer due to  $^{129}\text{Xe}$  HFC as a function of the lifetime of the Rb-Xe interaction events. Polarization transfer in long-lived VDW complexes was found to dominate over short-lived binary collisions in the investigated model conditions, the low gas temperature of  $T = 300$  K and the high pressure of  $p = 2.4$  bar. Furthermore, a model gas composition was used, where Xe adopted, in addition to being the target polarization reservoir, also the role of the buffer gas. This approximation is also used in the present work. Polarization transfer in single individual VDW molecules is more substantial than in single binary collisions, and the large number of binary collisions only partially changes this picture at the ensemble level, in this simplified model.

Upon detailed investigation of individual binary and VDW events, a stepwise polarization transfer to the xenon nucleus was found [20], arising from the steep increase of the magnitude of Xe HFC at small values of the internuclear distance  $R$  of the Rb-Xe pair. In the periodic bond-distance oscillations taking place in long-lived complexes, the steps constitute a staircase with the step height increasing in time. In some events, the VDW complex and the polarization transfer could sustain disturbing intrusions by third bodies (other Xe atoms in the simulation of Ref. 20) over a fairly long period, before the break-up of the complex eventually occurred.

After this initial simulation work, questions remain concerning the role of further physical interactions not included in Ref. 20, the trends in the polarization transfer events as a function of the experimental parameters  $T$  and  $p$ , and the effect of the detailed gas composition on the polarization transfer efficiency. In this article we tackle the first of these questions and find an important influence of the explicit incorporation of the nuclear spin  $\hat{I}$  of the  $^{85/87}\text{Rb}$  atom, in reducing the magnitude of spin exchange to Xe in the long-lived VDW complexes, as compared to the simulations of Ref. 20. This interaction is parameterized via the Rb HFC tensor  $\mathbf{A}_{\text{Rb}}$ , which remains practically constant and, compared to  $\mathbf{A}_{\text{Xe}}$ , strong in the range of values of the oscillating  $R(t)$  occurring in the VDW complexes. Consequently, the unpaired electron and the Rb nucleus constitute a strongly coupled, semi-isolated two-spin system, which is either transiently (in binary collisions) or quasi-periodically (in VDW complexes) perturbed by the HFC to the Xe nucleus. The desired polarization transfer to the Xe nucleus, provided by this perturbation, occurs as determined by Rabi-like oscillations governed by the electronic Zeeman and HFC interactions within the Rb atom. A simple analytical formula derived based on the event lifetime distribution and

the Rabi transition probabilities reveals that the spin-flip transition coupling to initial and final hyperfine states of Rb belonging to different total angular momentum branches is mainly responsible for the polarization transfer, at the simulated phase point.

Additionally, we include the effect of NQC to the Rb nucleus (parameterized via  $\mathbf{Q}_{^{85}\text{Rb}}$  or  $\mathbf{Q}_{^{87}\text{Rb}}$  for the corresponding  $K = 5/2$  and  $3/2$  isotopes, respectively), and the nuclear dipole-dipole coupling  $\mathbf{D}_{\text{Rb-Xe}}$ .

To meet all these ends, a new stand-alone simulation program was implemented in the Python language [33, 34] to propagate the spin density matrices in time. This happens in practice by extracting the Rb-Xe events and the corresponding time-dependent interatomic distances  $R(t)$  from a MD trajectory and numerically solving the Liouville-von Neumann (LVN) equation for the events, as driven by the time-dependent, QC-parameterized spin Hamiltonian  $\hat{H}[R(t)] \equiv \hat{H}(t)$ , followed by ensemble-averaging of the results.

## II. CALCULATIONS

### A. Molecular dynamics simulations

In the MD calculations, the instantaneous positions and velocities of the atoms were retrieved from a trajectory obtained on the NAMD code [35] by integrating the classical equations of motion. As previously [20], the simulation consisted of a Rb atom in the gas of 2196 Xe atoms, produced corresponding to  $T = 300$  K and  $p = 2.4$  bar over a 268-ns production time. A cubic simulation box with side length equal to 333.96 Å, was employed. This simulation represents a simplified model as compared to normal gas composition in SEOP polarization cells, in which  $\text{N}_2$  molecules and He atoms are found [5]. In the simulated conditions, most of the interatomic collisions, including the three-body events that are responsible for the formation and break-up of VDW complexes between Rb and Xe atoms, happen between the Xe atoms.

Rb-Xe interaction events were extracted from MD snapshots saved at even intervals ( $\Delta\tau = 50$  fs). We define collision events as Xe visitations inside a 9 Å radius from Rb, as it is beyond this distance that both the Rb-Xe radial distribution function and the parameters of the spin Hamiltonian take values corresponding to an infinite atomic separation [20]. The distribution of the number of these events in the present simulation conditions, reported in Ref. 20, is weighted towards short-lived binary collisions. Most collisions have a lifetime shorter than 25 ps, whereas the long-lived VDW complexes that are mainly responsible for the polarization transfer to  $^{129}\text{Xe}$ , are substantially more rare in the present conditions.

The gas composition and other conditions of the simulation are presently selected for modeling convenience. Whilst the present work concerns, similarly to Ref. [20], just a single pressure and temperature point (*vide supra*)

and the strongly simplified model of the SEOP gas mixture containing only Rb and Xe, we believe that the detailed features of the different kinds of binary and VDW events that are created, represent the real experimental situation. The latter typically [5] involves temperature in the range of 373...473 K, Rb density according to the latest liquid-state vapor pressure data [36] (meaning a lot fewer Rb per unit volume than presently), noble-gas partial pressure in the range of 0.03...0.15 bar, and gas admixture of the noble gas, N<sub>2</sub> and He, as well as Rb having a total pressure at 1...2 bar. We defer studies of the dependence of polarization transfer  $T$ ,  $p$ , and gas composition until further, currently ongoing work in our laboratory.

## B. Spin Hamiltonian

A time series of spin Hamiltonians for each event was obtained using pre-calculated tables of the parameters as functions of the Rb-Xe distance  $R$ . The basic spin Hamiltonian of one unpaired electron and one spin-1/2 nucleus in a Rb-Xe pair, used in Ref. [20],

$$\hat{H}_0(t) = \mu_B \hat{\mathbf{S}} \cdot \mathbf{g}(t) \cdot \mathbf{B} + \hat{\mathbf{S}} \cdot \boldsymbol{\varepsilon}(t) \cdot \mathbf{M} + h \hat{\mathbf{S}} \cdot \mathbf{A}_{\text{Xe}}(t) \cdot \hat{\mathbf{K}}, \quad (1)$$

contains the  $g$ -tensor ( $\mathbf{g}$ ) that parameterizes the Zeeman interaction of the unpaired electron with the external magnetic field  $\mathbf{B}$ , the  $\boldsymbol{\varepsilon}$  tensor standing for the electron spin-rotation coupling with the mechanical angular momentum  $\mathbf{M}$  of the Rb-Xe pair, and the Xe HFC tensor ( $\mathbf{A}_{\text{Xe}}$ ) for the interaction of the unpaired electron with the Xe nucleus, respectively. We use Curl's approximation [37] to obtain  $\boldsymbol{\varepsilon}$  from  $\mathbf{g}$ , and consider  $\mathbf{M}$  a classical variable [12] calculated on-the-fly from the MD trajectory. Among these terms, HFC to <sup>129</sup>Xe is known to be principally responsible for the polarization transfer [2], the Zeeman term suppresses the transfer upon increasing the field strength  $B$  [7, 8, 38], and the electron spin-rotation term was found to only have a little effect on the transfer in previous simulations [20]. Indeed the main consequence of the spin-rotation interaction has been to incur loss of Rb polarization, particularly in small-pressure experiments [19].

In the present work we make the spin Hamiltonian more realistic by extending it with additional terms as follows:

$$\begin{aligned} \hat{H}_1(t) = & \hat{H}_0(t) - \mu_N g_{\text{Rb}} \hat{\mathbf{I}} \cdot \mathbf{B} - \mu_N g_{\text{Xe}} \hat{\mathbf{K}} \cdot \mathbf{B} \\ & + h \hat{\mathbf{S}} \cdot \mathbf{A}_{\text{Rb}}(t) \cdot \hat{\mathbf{I}}. \end{aligned} \quad (2)$$

On the first row of Eq. (2),  $\mu_N g_{\text{Rb}/\text{Xe}} = \gamma_{\text{Rb}/\text{Xe}} \hbar$  include the  $g$ -factors parameterizing the nuclear Zeeman interaction, with  $\gamma$  the gyromagnetic ratios; we omit the small nuclear shielding effects. The second row contains the Rb HFC interaction, which couples  $\hat{\mathbf{S}}$  and  $\hat{\mathbf{I}}$  to constitute the total angular momentum of the Rb atom,  $\hat{\mathbf{F}}$ . This Hamiltonian is identical to that in Eq. (1) of Ref. 12, apart from

the fact that the electronic Zeeman, the electron spin-rotation, and the HFC interactions are in the present SD simulations employed in their full tensorial form. In particular, this means that we include what is, in the case of  $\mathbf{A}_{\text{Xe}}$ , termed as anisotropic spin exchange, in Ref. 39. Comparison with test simulations with isotropicized  $\mathbf{A}$  tensors indicated, however, a negligible effect of the non-isotropic contributions, in agreement with earlier calculations [39]. Therefore, the analysis of the time-dependent Schrödinger equation in Section III C (*vide infra*) was carried out using isotropic HFC tensors.

Pre-parameterization of the interaction tensors  $\mathbf{g}$  and  $\mathbf{A}_{\text{Rb}/\text{Xe}}$  was carried out by QC calculations at  $R$  ranging from 3 to 11 Å using fully relativistic density-functional theory (DFT) on the ReSpect code [40]. The hybrid PBE0 exchange-correlation functional [41] was used with, for both Xe and Rb atoms, the completeness-optimized [42], uncontracted 27s25p21d4f Gaussian basis set originally developed in Ref. 43, extended to four f-primitives in Ref. 44, and supplemented here with two sets of diffuse spd functions [45]. The QC results are tabulated in Tables S1 and S2 of the Supplemental Material [46]. The instantaneous values of the parameters were interpolated from the tables as needed in the SD simulation. Fig. 1 illustrates the dependence of  $\mathbf{A}_{\text{Xe}}$  and  $\mathbf{A}_{85/87\text{Rb}}$  on  $R$ .

## C. Spin dynamics simulations

A time series of spin Hamiltonians corresponding to instantaneous Rb-Xe distances  $R$ ,

$$\left\{ \hat{H}[R^\epsilon(n\Delta\tau)] \right\} \equiv \left\{ \hat{H}_n^\epsilon \right\}; \quad n = 1, \dots, N, \quad (3)$$

for each Rb-Xe interaction event  $\epsilon$  was used to drive the Hilbert-space evolution of the combined electron and nuclear spin density operator  $\hat{\rho}$  as

$$\hat{\rho}^\epsilon[(n+1)\Delta\tau] = e^{-(i/\hbar)\hat{H}_n^\epsilon\Delta\tau} \hat{\rho}^\epsilon(n\Delta\tau) e^{(i/\hbar)\hat{H}_n^\epsilon\Delta\tau}, \quad (4)$$

which realizes time propagation over the discrete MD snapshot intervals  $\Delta\tau$ . The event simulations were always initialized with a thermally polarized xenon nucleus

$$\hat{\rho}_K(0) = \frac{1}{2} \left( \hat{1} + \epsilon_K \hat{K}_z \right), \quad (5)$$

where the polarization level  $p_K = \langle \hat{K}_z \rangle / K = 2\langle \hat{K}_z \rangle = \epsilon_K/2$  and, at thermal equilibrium,  $\epsilon_K = \mu_N g_K B / (kT)$  involving the nuclear magneton  $\mu_N$ , the  $g$ -factor of <sup>129</sup>Xe,  $g_K$ , and the Boltzmann constant  $k$ . Each event  $\epsilon$  extracted from MD was, therefore, considered to represent a sub-ensemble of similar collisions, in which the <sup>129</sup>Xe spin polarization starts to evolve from a thermal equilibrium situation, instead of the pure  $m_S = \pm \frac{1}{2}$  states of an individual Xe nucleus. For the two-spin model in which the Rb nuclear spin is omitted, the initial density operator was  $\hat{\rho}^\epsilon(0) = |S, m_S\rangle \langle S, m_S| \otimes \hat{\rho}_K(0)$ , where

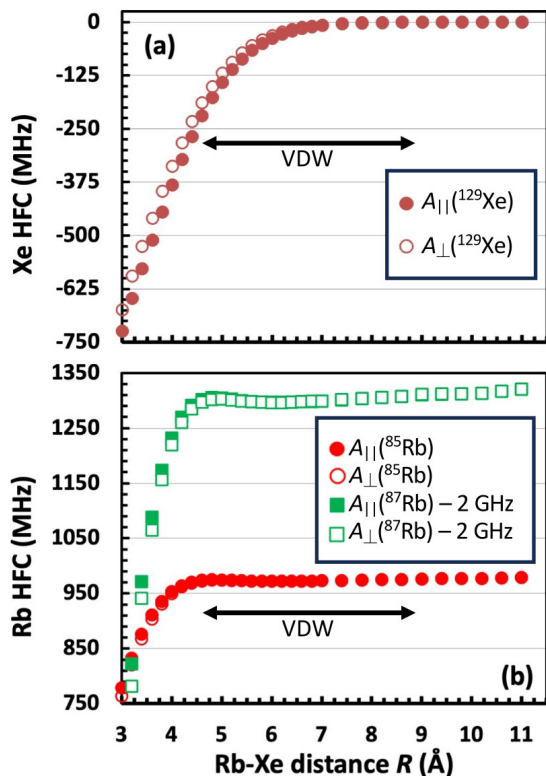


Figure 1. Calculated components of the HFC tensor  $\mathbf{A}(R)$  to (a)  $^{129}\text{Xe}$  and (b)  $^{85/87}\text{Rb}$  in an interacting Rb-Xe complex as functions of the internuclear distance  $R$ . The parallel ( $\parallel$ ) and perpendicular ( $\perp$ ) components with respect to the axis of the complex are shown as closed and open symbols, respectively. Note that the  $^{87}\text{Rb}$  data has been shifted down by 2 GHz for the purpose of illustration. The typical range of  $R$  in the oscillations of the Rb-Xe van der Waals (VDW) complexes is indicated by horizontal arrows.

the electron spin was initialized with the spin-up state with  $S = \frac{1}{2}, m_S = \frac{1}{2}$ . In the three-spin models involving the Rb nuclear spin, the events commenced from  $\hat{\rho}^\epsilon(0) = |F, m_F\rangle\langle F, m_F| \otimes \hat{\rho}_K(0)$  corresponding to full population of the coupled atomic  $F, m_F$  state with maximum alignment of the nuclear and electron spins, *i.e.*,  $F = 3, m_F = 3$  and  $F = 2, m_F = 2$  for  $^{85}\text{Rb}$  and  $^{87}\text{Rb}$  isotopes, respectively, resulting from optical pumping with  $\sigma^+$ -polarized light [47]. Assuming a fully polarized Rb atom in our simulations means that we deliberately neglect the rate of spin-destructing collisions of Rb with the other gas-phase species, in comparison with the optical pumping rate [48]. While this is in line with the focus of the present work on the details of the spin-exchange collisions, such depolarization processes are necessarily incorporated in holistic models of the entire SEOP process [24]. Presently a Xe atom always meets an initially favorably polarized Rb atom, which means that we also omit the Xe spin depolarization due to backwards transfer to Rb, on account of the Xe HFC interaction [5]. In reality this takes place, as the Rb polarization is typically somewhat less than unity.

The time dependence of the expectation value of the observable  $\hat{O}$ , *e.g.*, any of the Cartesian components of the electron or nuclear spins ( $\hat{S}_z, \hat{I}_z, \hat{K}_z$  etc.), can be obtained for each event from the time series of density operators as

$$\langle \hat{O}^\epsilon(n\Delta\tau) \rangle = \text{Tr} \left[ \hat{O} \hat{\rho}^\epsilon(n\Delta\tau) \right]. \quad (6)$$

In particular, the final polarization of the Xe spin pool is obtained as a sum, with  $\hat{O} = \hat{K}_z$ ,

$$\mathcal{K}_z = \sum_{\epsilon} \langle \hat{K}_z^\epsilon(N\Delta\tau) \rangle, \quad (7)$$

over the ensemble of Rb-Xe interaction events  $\epsilon$ . This realizes spin dynamics in which both the coherent and incoherent interactions are accounted for by the explicit time-dependence of the driving spin Hamiltonian in separate simulations of the events, which are subsequently averaged over.

Presently we focus on the polarization transfer to  $^{129}\text{Xe}$  nuclei in the collision events themselves and purposefully disregard relaxation effects of both the Rb atoms and xenon nuclei after each event. Xe relaxation will be incorporated in further work involving realistic composition of the SEOP gas mixture.

### III. RESULTS AND DISCUSSION

#### A. Simulated polarization of $^{129}\text{Xe}$ at $B = 1$ mT

We first discuss results for the polarization transfer at a typical SEOP field strength of 1 mT. Fig. 2 shows the average transfer to  $^{129}\text{Xe}$  in events belonging to the different lifetime categories, which range from short-lived binary collisions to long VDW events. Corresponding numerical data have been placed in Table S3 in the Supplemental Material [46]. Incorporation of the Rb HFC interaction term in the Hamiltonian, Eq. (2), results in a decline in the simulated polarization transfer to  $^{129}\text{Xe}$  in the important long-lived VDW events, which dominate in the present simulation conditions. Our simulation results, therefore, challenge the early view [15] that the role of the Rb HFC would be only limited to establishing the angular momentum coupling between  $\mathbf{S}$  and  $\mathbf{I}$ . In contrast, no effect can be seen in the binary collisions, which are in the present model of minor significance for the overall ensemble-averaged transfer to  $^{129}\text{Xe}$ . The fact that the incorporation of the Rb nuclear spin in the model has no effect in the picosecond timescale of the binary collisions, is in line with literature findings summarized in Ref. 24. In the VDW complexes, coupling to  $^{87}\text{Rb}$  entails an even larger decrease than to  $^{85}\text{Rb}$ , reflecting the more than three-fold strength of the HFC to the spin- $\frac{3}{2}$  isotope [Fig. 1(b)]. It will become apparent below, how this connection arises via Rabi-like oscillations within the Rb atom.

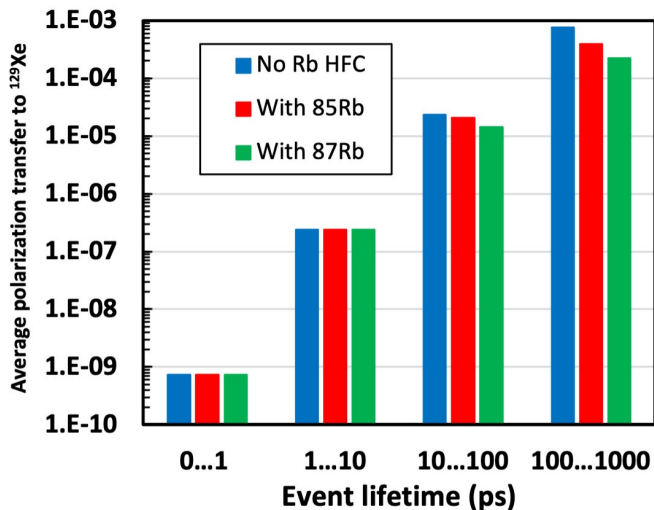


Figure 2. Simulated average polarization transfer,  $\langle p_{Xe}(N\Delta\tau) \rangle - p_{Xe}^{eq}$ , to  $^{129}\text{Xe}$  in Rb-Xe interaction events with different lifetime. Results shown with  $B = 1$  mT and the Hamiltonian  $H_1$  [Eq. (2)] with either no/ $^{85}\text{Rb}/^{87}\text{Rb}$  nuclear spin included. Note the logarithmic scale of the polarization transfer axis.

As compared to present findings, the experiments of Refs. 6 and 7 indicate a more important and, in the former case, an even dominating role of the binary collisions at pressures similar to the present 2.4 bar but at distinctly higher temperatures (75...200 C). Besides the temperature difference, the experiments of Ref. 7 were carried out at higher magnetic-field strengths, and in both cases in the presence of a buffer  $\text{N}_2$  gas. In the present, simplified simulation set-up practically all the interactions occur between Xe atoms, which have collision properties quite different from the experimentally often prevalent  $\text{N}_2$  molecules and/or He atoms. In particular, He and  $\text{N}_2$  are less efficient than Xe as third bodies in forming and breaking VDW complexes [15, 49]. This means that their incorporation into the model would most likely lengthen the lifetimes of the complexes and further increase their role in polarization transfer. In any case, the distribution of event types and lifetimes at the ensemble level cannot be expected to be entirely realistically reproduced in the present simulations, and must await for further work in the topic.

Detailed view of example VDW (Fig. 3) and binary events (Fig. S1 in the Supplemental Material [46]) as functions of time may be used to gain microscopic insight. A "clean" VDW event, unperturbed by intermediate third-particle interactions [Fig. 3(a)], displays the characteristic step-wise increase of  $^{129}\text{Xe}$  polarization [20], with each step synchronous with the occurrence of small Rb-Xe bond length  $R$  in the complex. It can be seen from Fig. 1(a) that the components of  $\mathbf{A}_{Xe}(R)$  are strongly modulated in the  $R$  range occurring during the oscillatory dynamics: A short interatomic distance corresponds to a large absolute value of Xe HFC. This lends a

natural explanation to the stepwise polarization increase. Fig. S1 [46] shows that, both in shallow and deep binary collisions, the single polarization transfer step occurs with indistinguishable effect of whether or not the Rb nuclear spin  $I$  is incorporated in the model. This is in agreement with earlier knowledge summarized in Ref. 24.

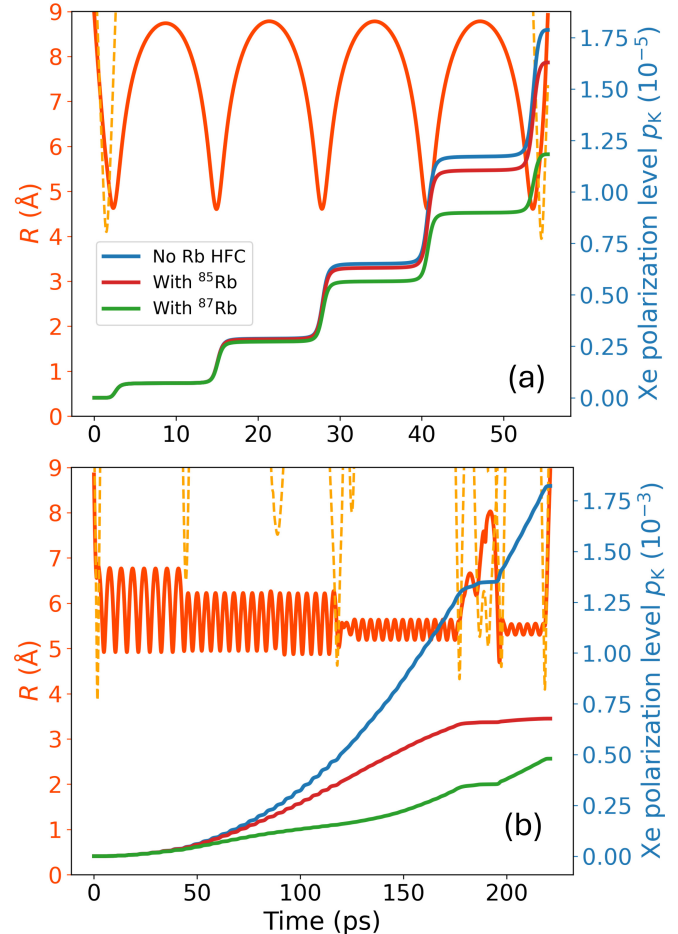


Figure 3. Nuclear spin polarization level of  $^{129}\text{Xe}$  ( $p_K$ ) in example (a) unperturbed and (b) perturbed Rb-Xe van der Waals complex, highlighting the effect of hyperfine coupling to  $^{85}/^{87}\text{Rb}$ . Conditions as in Fig. 2. The orange curve displays the Rb-Xe bond-length oscillation during the event [50]. The yellow dashed lines represent the distance to third bodies at the beginning and end of the complex lifetime, as well as [in (b)] in the intermediate perturbing events.

## B. Energy level structure

In the two-spin ( $S, K$ ) system, *i.e.*, when excluding the Rb nucleus, the polarization transfer to  $^{129}\text{Xe}$  takes place between the  $|\alpha_S\beta_K\rangle$  and  $|\beta_S\alpha_K\rangle$  states, where  $|\alpha\rangle$  and  $|\beta\rangle$  are the spin-up and -down Zeeman eigenstates of a  $S = \frac{1}{2}$ -particle. These states are intermixed by the

flip-flop operators contained in the Xe HFC Hamiltonian,

$$A_{\text{Xe}} \hat{S} \cdot \hat{K} = A_{\text{Xe}} \left[ \hat{S}_z \hat{K}_z + \frac{1}{2} (\hat{S}_+ \hat{K}_- + \hat{S}_- \hat{K}_+) \right], \quad (8)$$

where we, for simplicity, take  $A_{\text{Xe}}$  as isotropic, whilst the actual spin transfer simulations are done with full anisotropic detail. Fig. 4(a) illustrates schematically the dependence of the eigenvalues of  $\hat{H}_0$  at  $B = 1$  mT as functions of the Rb-Xe internuclear distance, at  $R = 9, 7$ , and  $5$  Å. In particular, the depicted energy levels contain the "secular"  $\hat{S}_z \hat{K}_z$  part of Xe HFC but omit the flip-flop parts within Eq. (8). The longest of these distances coincides with the onset of the Rb-Xe interaction event, at which the Xe HFC still has zero value, whereas  $R = 5$  Å corresponds to the closest interatomic distance occurring in the oscillation of a long-lived VDW complex. A diminishing Rb-Xe distance and, hence, increasing  $|A_{\text{Xe}}(R)|$  facilitate growing coupling strength, mixing and leading to spin transfer between the  $|\alpha_S \beta_K\rangle$  and  $|\beta_S \alpha_K\rangle$  states.

A realistic model for spin exchange contains also the Rb nuclear spin  $I$ . Without it, the height of the  $^{129}\text{Xe}$  polarization steps increases monotonically during the complex lifetime [20] [blue curve in Fig. 3(a)], whereas a slower increase of the step height is seen due to coupling to the  $^{85}\text{Rb}$  (red) or  $^{87}\text{Rb}$  (green) nucleus, respectively. In a longer VDW event [Fig. 3(b)], the steps are even seen to change into downward direction on account of the Rb HFC. Fig. 5 and S2 (the latter placed in the Supplemental Material [46]) illustrate the dynamics of  $p_S = \langle \hat{S}_z \rangle / S = 2 \langle \hat{S}_z \rangle$  and  $p_I = \langle \hat{I}_z \rangle / I$  in the same example events, indicating that the changes in these two variables are correlated with the Xe polarization steps. Compared to  $A_{\text{Xe}}$ , the Rb HFC is, on the one hand, stronger and, on the other hand, hardly at all modulated by VDW bond-length oscillations of typical amplitude [Fig. 1(b)]. Hence, the polarization changes of  $I$  occur without similar steps as in the case of Xe, as shown in Fig. S2(ab). Instead, a monotonic decrease of  $p_I$  starting from the initial unit value takes place during the lifetime of the Rb-Xe complex. In contrast, Fig. 5 indicates that the electron spin  $S$ , which is hyperfine coupled to the Xe spin, does show an initial downward step structure. Interestingly, during the phases of the VDW oscillations at which the Rb-Xe distance is large and  $p_K$  plateaus, some of the lost electron spin polarization is regained, and the steps in  $p_S$  display an upward slope at these points in time. For completeness, the simulated  $p_S$  in example deep and shallow binary collisions is illustrated in Fig. S3 in the Supplemental Material [46].

$S$  and  $I$  form a semi-isolated two-spin system for which, in the limit of vanishing Xe HFC (long  $R$ ), the natural starting point of the analysis is to couple  $\hat{S}$  and  $\hat{I}$  to the total spin  $\hat{F}$  of the Rb atom, with the  $|F m_F\rangle$  states [altogether  $2(2I + 1)$  of them] separated into the upper-energy branch of, for  $^{87}\text{Rb}$  ( $^{85}\text{Rb}$ ), five  $|2m_F\rangle$  (seven  $|3m_F\rangle$ ) states and the lower-energy branch of three  $|1m_F\rangle$  (five  $|2m_F\rangle$ ) states. Each of the states are split in two by HFC to the  $^{129}\text{Xe}$  ( $K = 1/2$ ) nucleus. The relevant

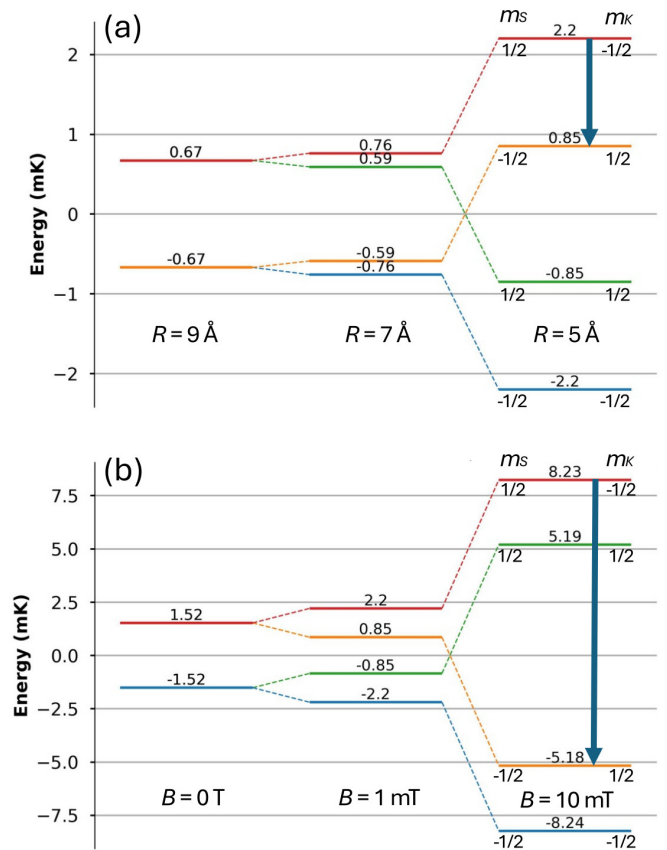


Figure 4. Energy eigenvalues (in units of mK) of the two-spin system consisting of the unpaired electron ( $S$ ) of the Rb atom and the  $^{129}\text{Xe}$  nucleus ( $K$ ), as functions of (a) the Rb-Xe distance at  $B = 1$  mT and (b) the magnetic-field strength at  $R = 5$  Å. The Hamiltonian  $\hat{H}_0$  of Eq. (1) was used without the small electron spin-rotation term, by using an isotropic Xe HFC, and including in the  $^{129}\text{Xe}$  HFC term only the secular  $A_{\text{Xe}} \hat{S}_z \hat{K}_z$  part. The two levels involved in the polarization transfer via the  $\hat{S}_- \hat{K}_+$  operator are joined by the vertical arrow. The  $m_S$  and  $m_K$  quantum numbers of the levels are indicated.

polarization transfer to  $^{129}\text{Xe}$  can now be viewed to occur via the  $\hat{S}_- \hat{K}_+$  operators stepping down the combined Rb-atom quantum number  $m_F$  ( $m_S$ ) and flipping up the  $^{129}\text{Xe}$  spin projection  $m_K$ .

Fig. 6 displays the energy-level structures of the three-spin models with  $^{87/85}\text{Rb}$ , again at  $R = 9, 7$ , and  $5$ -Å internuclear separation, prior to the application of the flip-flop operators of Xe HFC. The Figure illustrates the spin-flip couplings of the initial state 1, with  $F = 2, m_F = 2$  or  $F = 3, m_F = 3$  for  $^{87}\text{Rb}$  and  $^{85}\text{Rb}$  isotopes in this order, to two other states 2 and 3, occurring in the Rb-Xe events [13]. The first of these couplings occurs to state 2 within the same upper ( $F = 2$  or  $F = 3$ ) branch of hyperfine states as that of the initial state and has, therefore, a relatively low transition energy. The Xe HFC interaction only involves the  $\hat{S}_-$  and  $\hat{S}_+$  contributions to  $\hat{F}_-$  and  $\hat{F}_+$ . Hence, the  $F$  quantum number is not necessarily preserved and there is another coupling from state 1 to

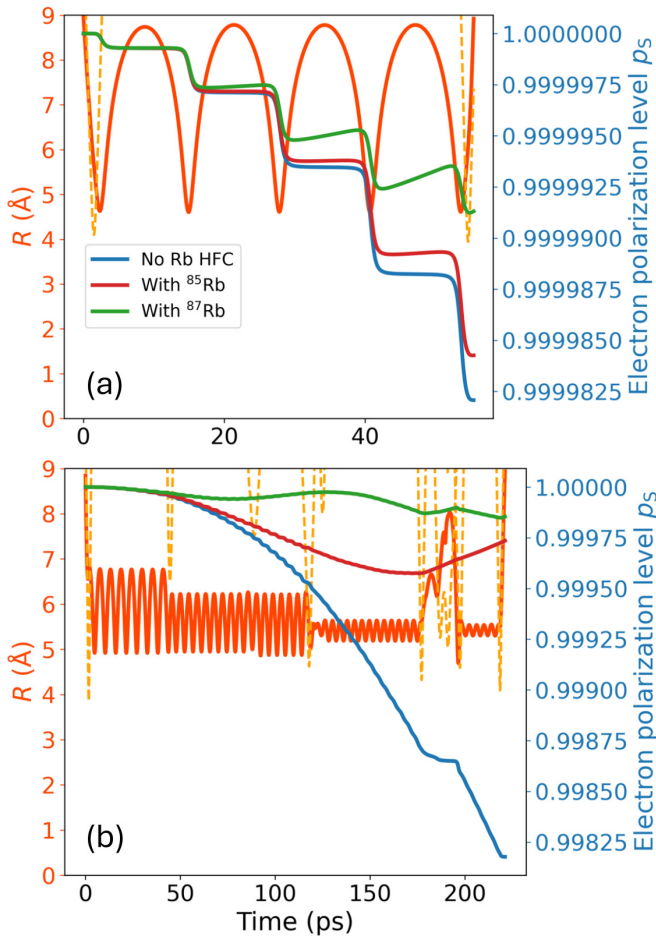


Figure 5. As Fig. 3 but for electron spin polarization level  $p_S$  in example (a) unperturbed and (b) perturbed Rb-Xe van der Waals complexes.

the lower  $F$  branch, to state 3.

### C. Numerical model of a van der Waals complex

It is relatively straightforward to numerically solve for the time-dependent Schrödinger equation (TDSE) for the present two- or three-state systems of the two- or three-spin models, respectively, under the simplifying assumption of sinusoidally time-dependent Rb-Xe bond-length oscillating in an unperturbed, long-lived VDW complex. The calculation gives the occupation probabilities of the initial state,  $P_1(t)$ , and the final states,  $P_2(t)$  and  $P_3(t)$ . The detailed procedure is described in the Supplemental Material [46]. The results for the simple 2-spin model (devoid of the Rb nuclear spin) are illustrated in Fig. 7 and those appropriate to the three-spin models involving the Rb nuclei, in Fig. 8.

The results for the two-spin model system [Fig. 7(a)] indicate, in the depicted timescale, a monotonically increasing transition probability for the three lowest magnetic-field values, from 0.1 to 10 mT. The occupation

of state 2, in which  $^{129}\text{Xe}$ , initially in the  $\beta$  state, has been flipped to  $\alpha$ , builds up to the value of 0.25% in the depicted 500 ps period, which is roughly twice the lifetime of the longest presently simulated VDW events. Superimposed upon the increasing transition probability there is a step-like pattern due to the oscillation of the Rb-Xe distance within the VDW event, with plateaus occurring in the phases of the periodic motion in which the Rb-Xe distance acquires large values and, correspondingly, the steps coinciding with a close proximity of the two atoms. Also the step height is increasing as a function of time, as discussed in Ref. 20, underlining that both the essential features seen in the spin dynamics simulation of the "clean" (unperturbed by third bodies) VDW events, at low  $B$ -values, are recovered by this simple model.

Fig. 7(b) illustrates the results of pursuing the propagation of the TDSE further, up to a 100-fold time interval as compared to Fig. 7(a). A periodic oscillatory pattern, with both the period and the value at the maxima decreasing as a function of  $B$ , emerges. This underlines that, within the realistic lifetime of a Rb-Xe VDW complex and at low field values, the polarization transfer to the Xe nucleus happens in the initial rising phase of the periodic oscillation, and is eventually cut short by the break-up of the VDW bond. With  $B$  there is a gradual decrease of the polarization step height and eventual turning over to downward steps, visible in the  $> 100$  mT curves in the depicted time scale.

As detailed in the Supplementary material [46], the slow dynamics can be identified as Rabi-like oscillation of the Rb electron spin between states 1 and 2, set in motion by the perturbing Xe nucleus and, for which, there exists a standard oscillatory solution given by the Rabi formula, in which both the oscillation amplitude and frequency are determined by factors  $\omega_{n1}$  and  $V_{n1}$  (with  $n = 2, 3$ ), the energy difference between the initial and final states, as well as the corresponding spin-flip perturbation, respectively. For the two-spin model, both the amplitude and the period appearing in the Rabi formula are in excellent agreement with the results of propagating the TDSE. At field strengths in the 10-mT range and above, the electron spin Zeeman interaction provides the dominant contribution to the oscillation frequency  $\omega_2 = \sqrt{\omega_{21}^2 + 4|V_{21}|^2}$  and, hence, determines the periodicity of the oscillation. At mT fields, the contribution of the  $^{129}\text{Xe}$  HFC, *i.e.*, the perturbation  $V_{21}$ , is comparable in magnitude.

Fig. 8 for the three-spin, three-level models shows the occupation probabilities of states 1-3, *i.e.*, the initial state 1 and the two final states 2 and 3, for the two Rb isotopes. Panels (a-c) present the  $^{87}\text{Rb}$  case and (d-f) stand for  $^{85}\text{Rb}$ . The occupation of state 1 decreases and that of state 2 increases monotonically with time, with the signature staircase of the VDW oscillation superimposed onto the curves. The long-time scale solutions of the TDSE, in the insets of panels (ab) and (de), are again characteristic of a Rabi-like oscillation between the states 1 and 2, which are in the same  $F = I + \frac{1}{2}$  branch of the manifold of Rb hyperfine states. Both the period and the

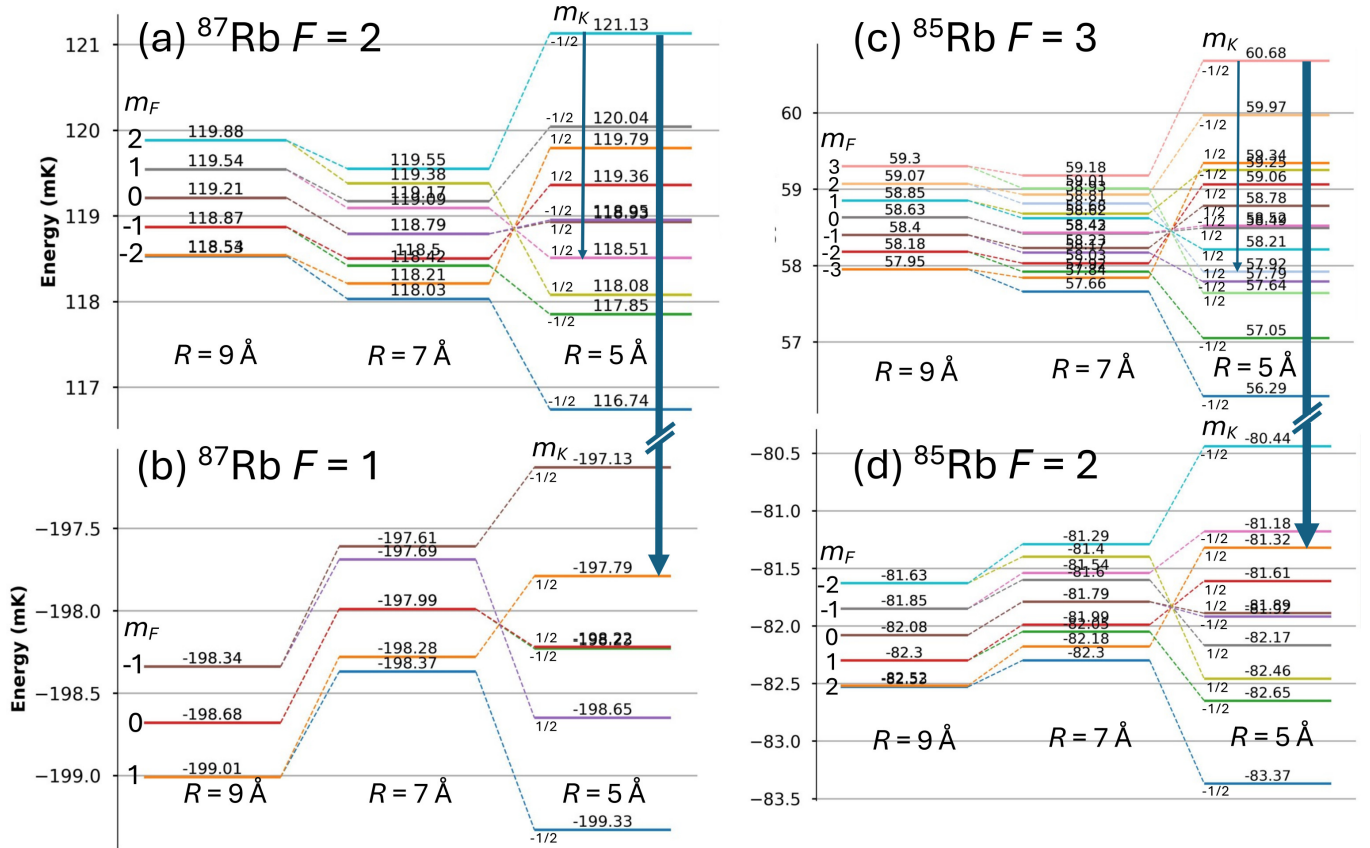


Figure 6. Energy eigenvalues (in units of mK) of the three-spin system consisting of the unpaired electron ( $S$ ) of the Rb atom, the Rb nuclear spin ( $I$ ) and the  $^{129}\text{Xe}$  nucleus ( $K$ ), as functions of the Rb-Xe distance at  $B = 1$  mT. (a) Upper-energy branch in case of  $^{87}\text{Rb}$  originating in the  $|2m_F\rangle$  states, (b) lower-energy branch in case of  $^{87}\text{Rb}$  originating in the  $|1m_F\rangle$  states, (c) upper-energy branch in case of  $^{85}\text{Rb}$  originating in the  $|3m_F\rangle$  states, and (d) lower-energy branch in case of  $^{85}\text{Rb}$  originating in the  $|2m_F\rangle$  states. The  $m_F$  quantum numbers of the coupled 2-spin system consisting of  $S$  and  $I$  are shown on the left for the levels at  $R = 9$  Å. The Hamiltonian  $\hat{H}_1$  of Eq. (2) was used without the electron spin-rotation term, by using an isotropic Xe HFC, and including in the  $^{129}\text{Xe}$  HFC term only the secular  $A_{\text{Xe}}\hat{S}_z\hat{K}_z$  part. The pairs of levels responsible for the polarization transfer via the  $\hat{S}_-\hat{K}_+$  operator are indicated by the vertical arrows, the thicknesses of which reflect the value of the matrix element  $|\langle i|\hat{S}_-\hat{K}_+|j\rangle|^2$ .

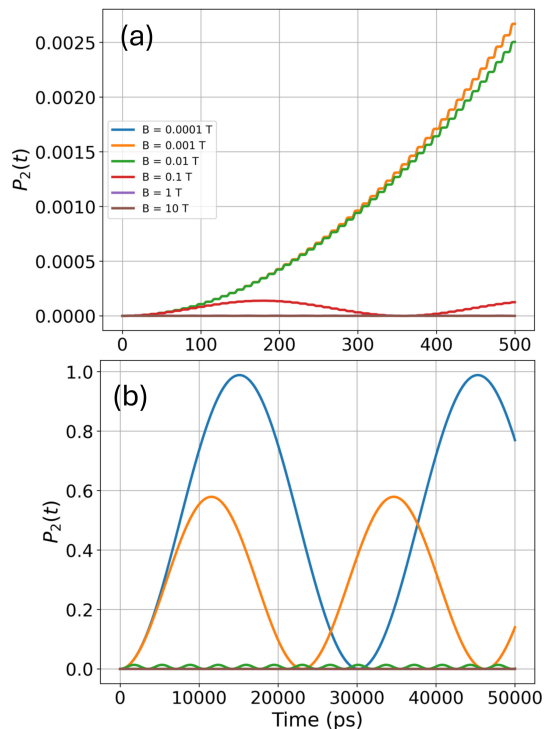


Figure 7. The final state occupation probability  $P_2$  as a function of time during the lifetime of a model VDW complex in the SEOP process in a two-spin model with electron and  $^{129}\text{Xe}$  nuclear spins. Results at different magnetic-field values are presented. Panel (b) illustrates a longer timescale evolution than what is depicted in (a).

amplitude of the oscillation agree well with the Rabi formula, using the calculated parameters in Table S4. The period of the oscillation of the two isotopomers are in the 40...50 ns range at the lowest fields. At the lowest considered field strengths, 0.1 and 1 mT, the theoretical maximum polarization transfer probabilities amount to about 0.6 and 0.4 for the three-spin models with  $^{87}\text{Rb}$  and  $^{85}\text{Rb}$ , respectively, but such large values can only be reached in individual Rb-Xe events extending to unrealistically long lifetimes. However, in view of the dominance of the comparatively few long-lived complexes in the overall polarization transfer in the present simulation (Fig. 2), increase in polarization may be only be gained by significantly extending the lifetime of the most persistent VDW complexes.

Similarly as in the simple two-spin model discussed above, at low field the frequency and period of the oscillation between the states 1 and 2 gain comparable contributions from both the energy difference  $\omega_{21}$  between the two states and the perturbation term  $4|V_{21}|$ . The distinct secular  $\hat{S}_z\hat{K}_z$  and the flip-flop  $\hat{S}_-\hat{K}_+$  terms of the Xe HFC [Eq. (8)] enter  $\omega_{21}$  and  $V_{21}$ , respectively. Upon increasing  $B$ , the energy difference term  $\omega_{21}$  (and the electron spin Zeeman contribution thereto), gradually start to play a dominant role in determining the oscillation frequency, with a concomitant, rapid decrease in the

amplitude of the maximum intra-branch transfer.

Fig. 8(c,f) shows that the probability of inter-branch transitions between states 1 and 3 (the latter in the  $F = I - \frac{1}{2}$  manifold) is non-zero and also displays the step structure characteristic of the oscillation of  $R$ , superimposed in this case over altogether third, periodic oscillation, which is slower than the time scale of the variation of the Rb-Xe distance but much faster than the  $1 \leftrightarrow 2$  intra-branch oscillation discussed above. As the sum  $\sum_{k=1-3} P_k = 1$ , the occupation of state 3 is reflected in  $P_1$  [panels (a,e)] as slow wiggles on top of the decaying occupation of state 1.

The Rabi formula, Eq. (S9), and the parameters in Table S4 are, again, applicable for this second prevailing Rabi-like oscillation, whose frequency is practically completely determined by the large energy difference  $\omega_{31}$  between the two states that belong to different hyperfine branches of the Rb atom. The oscillation has a period of 150...350 ps and below, at fields of 0.1 mT and above. Consequently, the maximum transition probability, of the order of  $10^{-3}$  and  $10^{-4}$  for  $^{87}\text{Rb}$  and  $^{85}\text{Rb}$  isotopes, respectively, can easily be reached within the accessible lifetime of the VDW complexes. The latter is maximally about 200 ps in the present simulation. Hence, the inter-branch  $1 \leftrightarrow 3$  transitions may play a significant practical role in the total polarization transfer, despite the much smaller amplitude of the oscillation of  $P_3$  as compared to that of  $P_2$ . Furthermore, the inter-branch oscillation amplitude obtains roughly five-fold larger maximum values in the model with the  $^{85}\text{Rb}$  isotope than in the case of  $^{87}\text{Rb}$ . This implies larger polarisation transfer for the lighter isotope, which is what one observes in the full simulation results in Figs. 2 and 3.

The oscillatory transition probabilities obtained from the numerical models indicate that, in contrast to the two-spin model that has two characteristic frequencies corresponding to the VDW bond-distance oscillation and a single Rabi-like oscillation largely arising from the electron spin-Zeeman interaction, the three-spin, three-level models are characterized by three frequencies. The slowest among them, that of the intra-branch oscillation of  $P_2$ , can be seen as the slowly varying envelope function over which the inter-branch oscillation in the state 3 occupation and the variation of the VDW bond distance can be identified. The step-like polarization transfer to  $^{129}\text{Xe}$  in the VDW complexes can be identified with the latter and, due to particularly the inter-branch transitions, the exact time of complex break-up is critical for the final polarization transfer in an individual event.

Fig. 9 illustrates the contributions of the intra- and inter-branch transitions for binary collisions [panel (a)] and VDW complexes (b). It is seen that within the short time scale of relevance to the binary collisions, and well into the lifetime range of the VDW complexes particularly for  $^{85}\text{Rb}$ , the inter-branch  $|\Delta F| = 1$  transitions provide the majority of the polarization transfer. Eventually, for very long-lived VDW complexes, the intra-branch  $\Delta F = 0$  transitions overtake. These findings

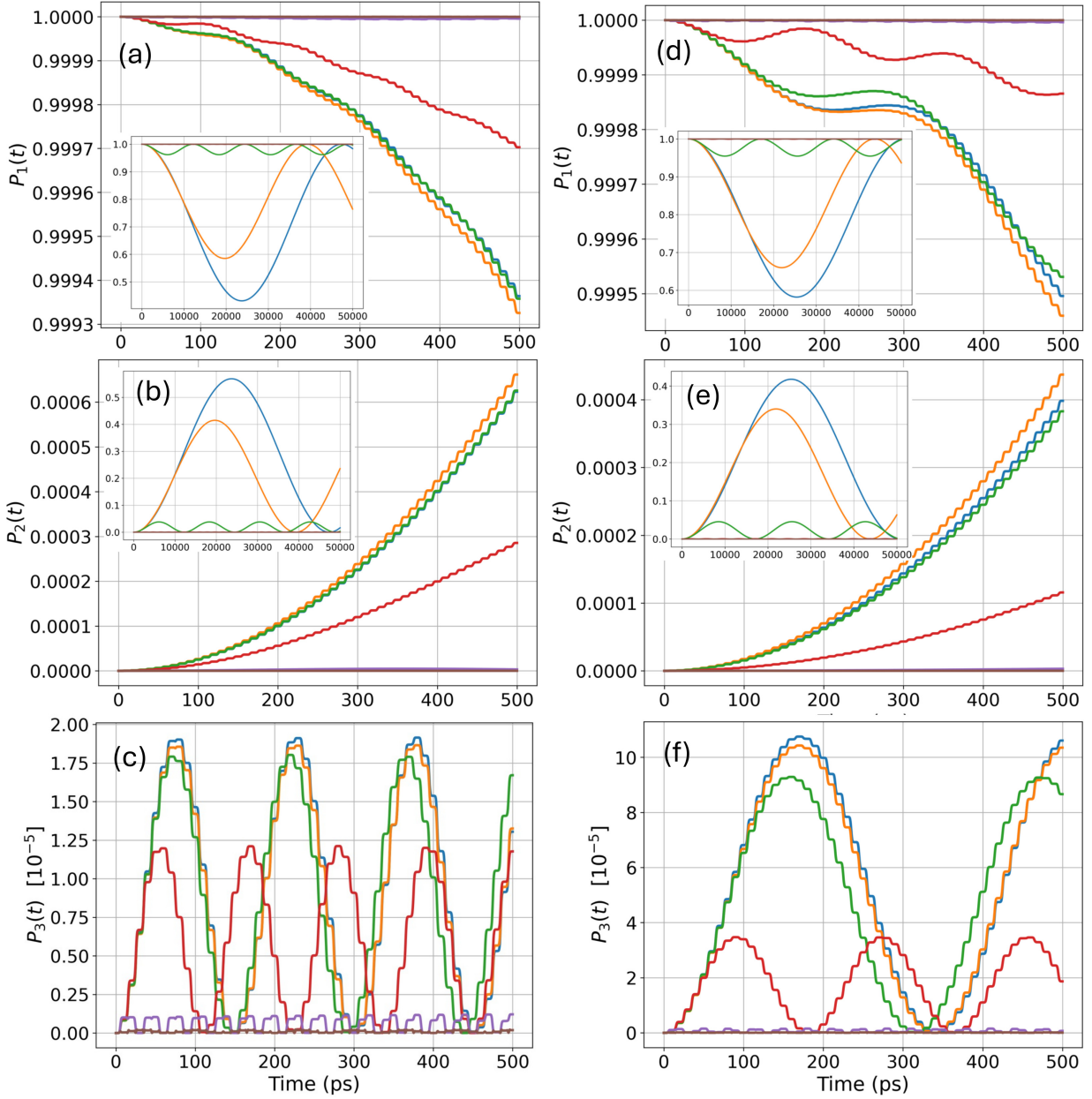


Figure 8. Transition probabilities as functions of time of the initial (a,d) and final (bc,ef) states of the Rb atom in an idealized unperturbed van der Waals complex with sinusoidal model for the Rb-Xe bond length. Panels (b,e) and (c,f) give probabilities for intra- and inter-branch transitions, respectively. Results from propagating the time-dependent Schrödinger equation for the three-spin models involving (a-c) the  $^{87}\text{Rb}$  and (d-f) the  $^{85}\text{Rb}$  isotope. The insets in panels (ab) and (de) expand the time axis to 50 ns.

parallel the discussion of the roles of the two kinds of transitions in Refs. [12, 13, 24].

Due to the slow oscillation of the occupation probability of the end states  $|2\rangle$  of the intra-branch transitions, aiming for exceedingly long-lived VDW complexes by conditions (*e.g.*, low gas pressure) that favor the existence of such VDW events [6, 51] may not eventually be the best way of optimizing the polarization level of the noble-gas nuclei. In contrast, events with average lifetime around the maximum of the inter-branch oscillation of  $P_3$  could be particularly useful for gaining efficient polarization transfer to  $^{129}\text{Xe}$ .

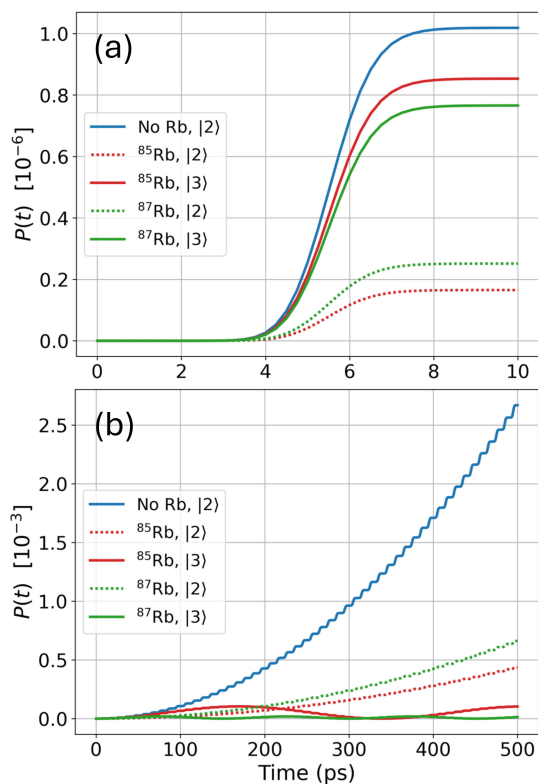


Figure 9. Transition probabilities to the different final hyperfine states in a spin-exchange event between Rb and  $^{129}\text{Xe}$ , from the propagation of the time-dependent Schrödinger equation at  $B = 1$  mT. Two different time scales are presented: (a) individual polarization step of relevance to binary collision events and (b) long VDW event. The model without Rb nucleus in blue. In models with  $^{85/87}\text{Rb}$  nuclear spins, the final state  $|2\rangle$  is in the same  $F = I + \frac{1}{2}$  branch as the initial state, and state  $|3\rangle$  is in the different ( $F = I - \frac{1}{2}$ ) branch.

Microwave-driven Rabi oscillations between the hyperfine states of Rb atoms, including alkali-alkali collision-induced decoherence effects thereto, have been investigated before (Ref. 52 and references therein). In the present case the oscillations take place between the combined hyperfine states of a Rb-Xe atomic pair undergoing inter-atomic dynamics in VDW complexes.

#### D. Magnetic-field dependence

Increasing  $B$  reduces the polarization transfer in VDW complexes [7–9, 12, 20, 38, 51, 53, 54], and this is what we find from the present simulations, too. In the model two-spin case, without the Rb nucleus  $I$ , the energy separation of the relevant  $|\alpha_S\beta_K\rangle$  and  $|\beta_S\alpha_K\rangle$  states increases with  $B$ , as shown in Fig. 4(b). The coupled pair of states constitutes a two-level system where the first state receives, to the leading order in perturbation theory, an admixture of  $H_{21}^{(1)}/\omega_{21}^{(0)}$  from the second state. Hence, it is easy to see that the perturbation  $\hat{H}_{21}^{(1)}$ , in this case the flip-flop operator belonging to the Xe HFC, is less capable of coupling the pair of states as  $\omega_{21}$  increases upon going to a stronger magnetic field. In the Rabi formula, Eq. (S9), the increase of  $\omega_{21}$  leads both to a decrease of the oscillation amplitude and shortening of its period. These factors determine the gross features of the time evolution of the polarization transfer [see Fig. 7(a)].

Fig. 10 shows the simulated magnetic field-dependence of the polarization transfer for both the two-spin model and the more realistic three-spin systems, the latter with  $^{87}\text{Rb}$  and  $^{85}\text{Rb}$  nuclei in place. The figure presents the results for the longest-lived VDW complexes, with lifetime in the range 100...1000 ps. The corresponding data for all the lifetime categories are listed in Table S5 of the Supplemental Material [46]. Besides the overall lower level of transfer than in the two-spin model, another notable difference brought by  $I$  in the case of the VDW complexes is that Rb HFC helps to sustain the level of transfer obtained at low field up to a somewhat higher value of the field, than without the Rb HFC. Table S5 [46] indicates that, despite the overall reduction, the polarization transfer in binary collisions, which contribute to both the  $\tau = 0 \dots 1$  ps and  $\tau = 1 \dots 10$  ps lifetime categories in the Table, anyway persists much better upon increase of  $B$ , as compared to VDW complexes. This finding agrees with earlier knowledge [7–9].

These findings are backed also by the long-time scale results from the numerical TDSE model in Fig. 7(b) for the two-spin model (one Rabi-like oscillation) and in the insets of Fig. 8(ab,de) for the three-spin models (two oscillations). The oscillation amplitude decays more rapidly with increasing  $B$  in the two-spin model than in the more realistic three-spin models. The magnetic-field dependence of the energy levels of the three-spin systems are illustrated in Figs. S5 and S6 in the Supplemental Material for  $^{87}\text{Rb}$  and  $^{85}\text{Rb}$ , respectively. The relevant transition energy  $\omega_{21}$  is dominated by the electronic Zeeman term both in the model without the Rb spin and in the intra-branch transition of the three-spin models. Hence,  $\omega_2$  grows approximately linearly with  $B$  and limits the amplitude of the relevant Rabi oscillation and polarization transfer. In contrast, the  $\omega_{31}$  parameter of the inter-branch oscillations of the three-spin models continues to be dominated by the Rb HFC up to the relatively

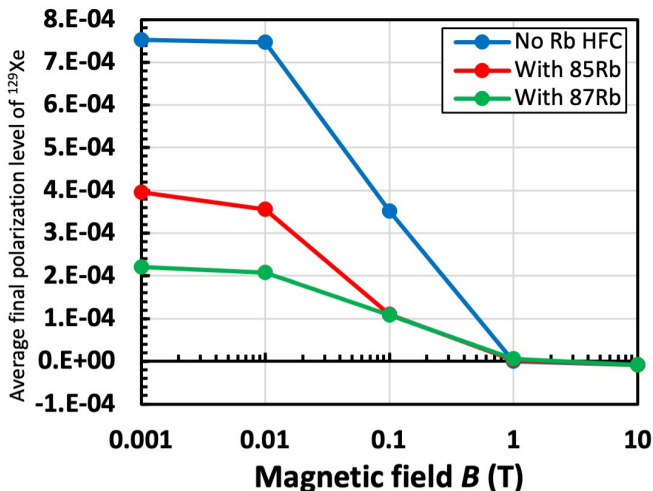


Figure 10. Average final  $^{129}\text{Xe}$  polarization at the end of the Rb-Xe interaction events as a function of magnetic-field strength, for the most important, long-lived VDW complexes, with lifetime more than 100 ps. Results are shown without HFC to the Rb nucleus and with coupling to  $^{85}\text{Rb}$  and  $^{87}\text{Rb}$ .

large 100-mT field strength, which renders the realistic three-spin models more resilient to increasing  $B$ , than the model in which  $I$  is omitted.

Increasing  $B$  decreases the transition probability and a dramatic change happens between 10 and 100 mT. Starting from the latter field strength only a modest polarization transfer can be seen in the simulated timespan. This is in qualitative agreement with the experimentally known suppression of the VDW contribution to the polarization transfer at field strengths beyond 10 mT [53, 54], which leaves the binary collisions as the dominating mechanism at high fields. The data of Bhaskar *et al.* [53] show an increasingly broad plateau of the polarization transfer at the low-field limit, with increasing sample pressure. Our high-pressure simulation is consistent with this observation. A detailed comparison of the magnetic-field dependence results from our simplified simulation with the low-pressure experimental data of Refs. 53 and 15 is, however, not feasible. Upon reaching the field strength of 10 T, practically no transfer to  $^{129}\text{Xe}$  takes presently place either with or without Rb HFC, *i.e.*, xenon remains at its thermal equilibrium polarization level in both cases.

### E. Further interactions

As the relevant Rb isotopes are quadrupolar, it is of interest to also investigate polarization transfer in models that account for the possible effects of the NQC interaction of the quadrupole moment of the alkali-metal nucleus with the electric field gradient (EFG) at the Rb nuclear site. The latter is generated in the collision events with the  $^{129}\text{Xe}$  atom, in which the spherical symmetry of the

atom is broken. The Hamiltonian becomes in this case

$$\hat{H}_2(t) = \hat{H}_1(t) + h\hat{I} \cdot \mathbf{Q}_{\text{Rb}}(t) \cdot \hat{I}, \quad (9)$$

for which  $\mathbf{Q}_{\text{Rb}}$  was parametrized for both  $^{87}\text{Rb}$  and  $^{85}\text{Rb}$  by calculating the EFG employing scalar-relativistic second-order Douglas-Kroll-Hess (DKH2) theory [55] and basis without the diffuse spd functions, on the ORCA code [56], with the other details as described above. The calculated  $\mathbf{Q}_{\text{Rb}}$  as a function of the Rb-Xe distance is listed in Table S2 in the Supplemental Material [46]. Furthermore, the direct internuclear dipole-dipole (DD) coupling Hamiltonian was added as

$$\hat{H}_2'(t) = \hat{H}_1(t) + h\hat{I} \cdot \mathbf{D}_{\text{Rb-Xe}}(t) \cdot \hat{\mathbf{K}}, \quad (10)$$

where  $\mathbf{D}_{\text{Rb-Xe}}(t)$  is straightforwardly obtained from the atomic positions. Results of the polarization transfer simulations in the presence of, on the one hand, the Rb NQC and, on the other hand, DD coupling, are listed at  $B = 1$  mT in Table S3 [46]. As the changes in the polarization transfer due both the DD coupling and Rb NQC appear only starting from the third significant digit in the longest-lifetime event category, these interactions can safely be omitted from the present consideration.

### F. Analytical model of polarization transfer

As discussed above, the gross features of the polarization transfer to  $^{129}\text{Xe}$  are, in the model VDW complex, governed by the transition probabilities that undergo Rabi-like oscillations between the initial, fully polarized atomic state of Rb and the two final states in either the same or different branch of the hyperfine states of the alkali metal atom. This suggests that one may arrive at a potentially useful semianalytical formula for the polarization transfer within the long-lived VDW complexes. Indeed, if we know the lifetime distribution  $\mathcal{N}(\tau)$  of such events, the total polarization in them can be approximated as [46]

$$\mathcal{K}_z = \int_0^\infty \mathcal{N}(\tau) \left[ P_2(\tau) + P_3(\tau) - \frac{1}{2} \right] d\tau, \quad (11)$$

where the intra- and inter-branch transition probabilities,  $P_2$  and  $P_3$ , have been represented with the appropriate Rabi formula, Eq. (S9). Assuming, for simplicity, an exponentially decaying lifetime distribution [12],

$$\mathcal{N}(\tau) = \frac{N_t}{\tau_0} \exp(-\tau/\tau_0), \quad (12)$$

with  $N_t$  equal to the total number of such events, one obtains for the polarization transfer

$$\Delta\mathcal{K}_z = 2N_t\tau_0^2 \left( \frac{|V_{21}|^2}{1 + \omega_2^2\tau_0^2} + \frac{|V_{31}|^2}{1 + \omega_3^2\tau_0^2} \right), \quad (13)$$

with the Rabi parameters  $V_{i1}$  and  $\omega_i$  ( $i = 2, 3$ ). On the other hand,  $N_t$  may be equated to the product  $Z\Delta t$

of the rate  $Z$  of forming VDW complexes and the total polarization time  $\Delta t$ . This gives the approximate total polarization transfer per unit time as

$$\frac{\Delta\mathcal{K}_z}{\Delta t} = 2Z\tau_0^2 \left( \frac{|V_{21}|^2}{1 + \omega_2^2\tau_0^2} + \frac{|V_{31}|^2}{1 + \omega_3^2\tau_0^2} \right). \quad (14)$$

The resulting total polarization transfer rates are displayed in Fig. 11, using the values applicable to the present simulations. In particular, we used  $\tau_0 = 24$  ps based on fitting Eq. (12) to the current event lifetime distribution, including VDW events with lifetimes in excess of 15 ps. While  $\tau_0$  is close to the empirical value [9, 15] given for a pure Xe sample at the present density, the limited statistics causes it to be only considered an order-of-magnitude estimate. Indeed, in a realistic gas composition involving also  $N_2$  and/or He, the average complex lifetime is expected to increase [15, 24, 49] as compared to our Xe-only model system.

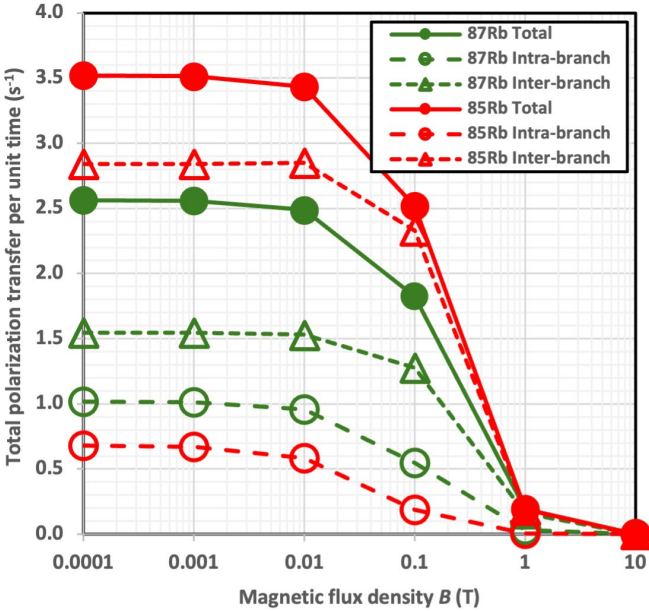


Figure 11. The roles of inter- and intra-branch transitions in the total polarization transfer per unit time for both  $^{87}\text{Rb}$ - $^{129}\text{Xe}$  and  $^{85}\text{Rb}$ - $^{129}\text{Xe}$  systems, according to Eq. (14).

Comparing with the simulated magnetic-field dependence of the polarization transfer in Fig. 10, we see that the results of the simplified model in Fig. 11 reproduce the overall trend qualitatively. Maximum, practically constant transfer is obtained at low field values in the range of mT strength, and a decrease in transfer takes place at higher field strengths. Furthermore, transfer is stronger with the  $^{85}\text{Rb}$  isotope than with  $^{87}\text{Rb}$ . The decrease at high  $B$  takes place at similar field values as in the simulation results.

The most important qualitative message of the results of Fig. 11 is in the relative contributions of the intra- and inter-branch spin-flip transitions, which are described via

their own Rabi-like oscillations and give rise to the two terms in Eq. (14). It is seen that, in the present lifetime range of the long-lived VDW complexes characterized by the value of  $\tau_0$  around 24 ps and for  $^{85}\text{Rb}$ , the inter-branch transitions are, indeed, responsible for the majority of polarization transfer across the favorable field-strength range in Fig. 11. This happens despite the much smaller amplitude of the relevant inter-branch oscillation. For  $^{87}\text{Rb}$ , the intra-branch contribution to the total transfer approaches the magnitude of the inter-branch contribution.

As evident from the above, the reason for the strong contribution of the  $|\Delta F| = 1$  transitions is the fact that the associated oscillation of the final-state occupation probability has sufficient time to reach maximum value in the accessible complex lifetime, whereas the longer-period intra-branch oscillation does not. This finding underlines the importance of the inter-branch spin-flip transitions. The relative contributions are sensitive, however, to the value of  $\tau_0$ , with the inter- and intra-branch transitions dominating short- and long-lifetime events, correspondingly.

### G. Relation to experiment

In principle, to compare with the experimental spin-exchange cross section  $\sigma_{\text{SE}}$  [12], we may relate the present work to Eq. (24) of Ref. 24, the rate equation for the  $^{129}\text{Xe}$  polarization:

$$\frac{dp_K}{dt} = [\text{Rb}]\sigma_{\text{SE}}(p_S - p_K) - \Gamma p_K, \quad (15)$$

where  $[\text{Rb}]$  and  $\Gamma$  are the Rb number density and intrinsic Xe relaxation rate, respectively. We equate

$$\frac{dp_K}{dt} \approx 2 \frac{\Delta\mathcal{K}_z}{\Delta t}$$

and, upon omitting the relaxation term and approximating  $p_S - p_K \sim 1$ , one gets from Eq. (14)

$$\sigma_{\text{SE}} \approx \frac{4Z\tau_0^2}{[\text{Rb}]} \left( \frac{|V_{21}|^2}{1 + \omega_2^2\tau_0^2} + \frac{|V_{31}|^2}{1 + \omega_3^2\tau_0^2} \right). \quad (16)$$

Using values from the present simulation,  $[\text{Rb}] \sim 3 \times 10^{22} \text{ m}^{-3}$  and  $Z \sim 3 \times 10^9 \text{ s}^{-1}$ , we arrive at the total cross section value of  $\sigma_{\text{SE}} \sim \mathcal{O}(10^{-18}) \text{ m}^3/\text{s}$  corresponding to the low-field plateau region of Fig. 11. Such a value overestimates the experimental  $\sigma_{\text{SE}}$  results pertinent to VDW complexes [24] by three orders of magnitude. The underlying reasons for the large values obtained in the model of Eq. (14) include our model gas composition in which  $[\text{Xe}]$  (and, hence,  $Z$ ) is 1–2 orders of magnitude too large as referenced to the standard SEOP conditions. Furthermore, Xe relaxation is omitted in this model and Eq. (13) assumes VDW complexes unperturbed by 3<sup>rd</sup>-body events that slow down

polarization transfer [Fig. 3(b)]. The TDSE model, on which Fig. 11 is based, also altogether neglects the effects of electron spin-rotation interaction, which serves as a channel for Rb relaxation that competes with polarization transfer to Xe [11, 12].

If one, instead of the TDSE model and Eq. (16), employs the polarization transfer  $\Delta p_K$  from the present multiscale spin dynamics simulations (see the numerical data in Table S5),  $\sigma_{SE}$  around  $50 \times 10^{-21}$  (with  $^{85}\text{Rb}$ ) and  $30 \times 10^{-21} \text{ m}^3/\text{s}$  ( $^{87}\text{Rb}$ ) follow for VDW complexes from the application of Eq. (15), still neglecting relaxation and, due to assuming a complete polarization of the Rb atom at the beginning of each interaction event with Xe, omitting also the polarization back-flow from Xe to Rb. These spin dynamics simulation results overestimate the experimental  $\sigma_{SE}$  listed by Kelley and Branca [24] currently by an order of magnitude.

As stated above, the present simulations are principally targeted at producing examples of Rb-Xe interaction events of different lifetimes, and analyzing the details of the polarization transfer within them. It is in this vein that also the semianalytical polarization transfer model of Eq. (14) is devised, based on the oscillatory character of the intra- and interbranch spin-flip transitions responsible for the polarization transfer. Eventually, for the type of multiscale spin dynamics modelling of the macroscopic polarization transfer, or an analytical model parameterized on its basis, to have quantitative predictive value, considerably improved statistics of the event lifetime distribution, as well as the intermolecular interactions of the Rb and Xe atoms will be needed. We also remind that the present models only concern the polarization transfer process in the Rb-Xe events, whilst Xe polarization loss via relaxation effects [21, 48] are disregarded.

All these aspects can eventually be explored when more extended MD simulations of realistic gas composition in SEOP processes, as well as the gas-phase relaxation rate  $T_1^{-1}$  of the  $^{129/131}\text{Xe}$  isotopes involving all known intrinsic mechanisms become available as a result of ongoing work in our laboratory. At that point a justified comparison with experimental spin-exchange cross sections should become feasible, and with that also the investigation of the exponential polarization build-up curve, the rate of which is empirically determined by the two parameters  $\sigma_{SE}$  and  $T_1^{-1}$  [48, 57].

#### IV. CONCLUSIONS

We have carried out a multiscale simulation of polarization transfer from optically polarized  $^{85/87}\text{Rb}$  to the nuclear spin of  $^{129}\text{Xe}$  in the spin-exchange collisions that occur in the SEOP method. The calculations employed a combination of molecular dynamics simulation of atomic trajectories in the gas phase, quantum-chemical construction of the time series of spin Hamiltonians for the Rb-Xe collision events extracted from the trajectories, and explicit spin dynamics simulation of the inter-

action events. In comparison with earlier work we have now included explicitly the Rb nuclear spin and identified the transitions in the hyperfine spectrum of the alkali-metal atom that are responsible for the xenon nuclear spin flips. In addition to the multiscale simulation, we constructed an artificial, simple van der Waals complex, for which we explicitly solved the time-dependent Schrödinger equation including the relevant states.

We find a stepwise build-up of  $^{129}\text{Xe}$  spin polarization in individual collisions when the Rb-Xe distance is small, due to the steep interatomic distance dependence of Xe hyperfine coupling in the oscillations of the van der Waals complex. In contrast, the Rb hyperfine coupling remains practically constant in the interatomic distance range accessible in the collision events. The majority of the polarization transfer takes place in the long-lived van der Waals complexes in the presently simulated model, at a single temperature and pressure and a simplified gas composition.

Incorporation of the realistic three-spin model with  $^{85/87}\text{Rb}$  nuclear spin reduces the polarization transfer to  $^{129}\text{Xe}$ , as compared to the simple two-spin model with only electron and  $^{129}\text{Xe}$ . In the long-lived van der Waals complexes the polarization transfer steps are superimposed over long-period oscillations of the perturbed Rb atom. There are two distinct oscillations corresponding to the electron- $^{129}\text{Xe}$  spin-flip transitions due to the xenon hyperfine interaction coupling the initial, fully polarized state of the Rb atom to two possible final states in either the same or the other branch of the hyperfine spectrum. The former final state corresponds to very slow oscillation of the final-state occupation probability, with period exceeding the realistic lifetime of the van der Waals complexes. In contrast, the inter-branch oscillations are significantly faster and found to give an important contribution to the polarization transfer, as seen from a simple empirical model derived from the assumed event lifetime distribution and the Rabi oscillation model.

We expect that the present findings contribute to the understanding of basic physics of the polarization transfer process in spin-exchange optical pumping and eventually aid in practical optimization of the pumping set-ups. To the latter end, we are in ongoing work carrying out molecular dynamics simulations of more realistic gas mixtures involving also helium and nitrogen, and at a range of pressure and temperature points. Furthermore, polarization of also the quadrupolar  $^{131}\text{Xe}$  isotope is under investigation.

#### ACKNOWLEDGMENTS

The authors acknowledge useful discussions with Dr. Rajgowrav Cheenikundil (Oulu). Funding from Jenny and Antti Wihuri foundation and the University of Oulu Graduate School is appreciated (P.H.). Financial support has also been obtained from the University

of Oulu (Kvantum Institute), the Academy of Finland (projects 296292, 331008, and 361326). Computational

resources due to CSC—IT Center for Science (Espoo, Finland) were used.

- 
- [1] M. H. Levitt, *Spin Dynamics: Basics of Nuclear Magnetic Resonance* (Wiley, Chichester, 2001).
- [2] T. G. Walker and W. Happer, *Rev. Mod. Phys.* **69**, 629 (1997).
- [3] B. M. Goodson, *J. Magn. Reson.* **155**, 157 (2002).
- [4] T. R. Gentile, P. J. Nachter, B. Saam, and T. G. Walker, *Rev. Mod. Phys.* **89**, 045004 (2017).
- [5] J. Eills, D. Budker, S. Cavagnero, E. Y. Chekmenev, S. J. Elliott, S. Jannin, A. Lesage, J. Matysik, T. Meersmann, T. Prisner, J. A. Reimer, H. Yang, and I. V. Koptiyug, *Chem. Rev.* **123**, 1417 (2023).
- [6] G. D. Cates, R. J. Fitzgerald, A. S. Barton, P. Bogorad, M. Gatzke, N. R. Newbury, and B. Saam, *Phys. Rev. A* **45**, 4631 (1992).
- [7] Y.-Y. Jau, N. N. Kuzma, and W. Happer, *Phys. Rev. A* **66**, 052710 (2002).
- [8] Y.-Y. Jau, N. N. Kuzma, and W. Happer, *Phys. Rev. A* **67**, 022720 (2003).
- [9] M. A. Bouchiat, J. Brossel, and L. C. Pottier, *J. Chem. Phys.* **56**, 3703 (1972).
- [10] C. H. Volk, T. M. Kwon, and J. G. Mark, *Phys. Rev. A* **21**, 1549 (1980).
- [11] N. D. Bhaskar, W. Happer, and T. McClelland, *Phys. Rev. Lett.* **49**, 25 (1982).
- [12] W. Happer, E. Miron, S. Schaefer, D. Schreiber, W. A. van Wijngaarden, and X. Zeng, *Phys. Rev. A* **29**, 3092 (1984).
- [13] S. Appelt, A. B. Baranga, C. J. Erickson, M. V. Romalis, A. R. Young, and W. Happer, *Phys. Rev. A* **58**, 1412 (1998).
- [14] R. M. Herman, *Phys. Rev.* **137**, A 1062 (1965).
- [15] X. Zeng, Z. Wu, T. Call, E. Miron, D. Schreiber, and W. Happer, *Phys. Rev. A* **31**, 260 (1985).
- [16] T. V. Tscherebul, P. Zhang, H. R. Sadeghpour, and A. Dalgarno, *Phys. Rev. Lett.* **107**, 023204 (2011).
- [17] Z. Wu, T. G. Walker, and W. Happer, *Phys. Rev. A* **54**, 1921 (1985).
- [18] T. G. Walker, J. H. Thywissen, and W. Happer, *Phys. Rev. A* **56**, 2090 (1997).
- [19] I. A. Nelson and T. G. Walker, *Phys. Rev. A* **65**, 012712 (2001).
- [20] J. Rantaharju, M. Hanni, and J. Vaara, *Phys. Rev. A* **102**, 032813 (2020).
- [21] B. Saam, in *Hyperpolarized Xenon-129 Magnetic Resonance. Concepts, Production, Techniques and Applications*, T. Meersmann and E. Brunner (eds.) (Royal Society of Chemistry, 2015), p. 122.
- [22] Z. Wu, *Rev. Mod. Phys.* **93**, 035006 (2021).
- [23] K. F. Stupic, Z. I. Cleveland, G. E. Pavlovskaya, and T. Meersmann, *J. Magn. Reson.* **208**, 58 (2011).
- [24] M. Kelley and R. T. Branca, *J. Appl. Phys.* **129**, 154901 (2021).
- [25] A. Fink, D. Baumer, and E. Brunner, *Phys. Rev. A* **72**, 053411 (2005).
- [26] G. Norquay, S. R. Parnell, X. Xu, J. Parra-Robles, and J. M. Wild, *J. Appl. Phys.* **113**, 044908 (2013).
- [27] M. S. Freeman, K. Emami, and B. Driehuys, *Phys. Rev. A* **90**, 023406 (2014).
- [28] J. G. Skinner, K. Ranta, N. Whiting, A. M. Coffey, P. Nikolaou, M. S. Rosen, E. Y. Chekmenev, P. G. Morris, M. J. Barlow, and B. M. Goodson, *J. Magn. Reson.* **312**, 106686 (2020).
- [29] G. M. Schrank, arXiv:1911.015742v2.
- [30] J. W. Plummer, K. Emami, A. Dummer, J. C. Woods, L. L. Walkup, and Z. I. Cleveland, *J. Magn. Reson.* **320**, 106845 (2020).
- [31] M. Kelley, A. Burant, and R. T. Branca, *J. Appl. Phys.* **128**, 144901 (2020).
- [32] O. Katz, R. Shaham, and O. Firstenberg, *PRX Quantum* **3**, 010305 (2022).
- [33] <https://www.python.org/>.
- [34] C. R. Harris, K. J. Millman, S. J. van der Walt, R. Gommers, P. Virtanen, D. Cournapeau, E. Wieser, J. Taylor, S. Berg, N. J. Smith, R. Kern, M. Picus, S. Hoyer, M. H. van Kerkwijk, M. Brett, A. Haldane, J. Fernández del Río, M. Wiebe, P. Peterson, P. Gérard-Marchant, K. Sheppard, T. Reddy, W. Weckesser, H. Abbasi, C. Gohlke and T. E. Oliphant, *Nature* **585**, 357 (2020).
- [35] J. C. Phillips, R. Braun, W. Wang, J. Gumbart, E. Tajkhorshid, E. Villa, C. Chipot, R. D. Skeel, L. Kalé, and K. Schulten, *J. Comput. Chem.* **26**, 1781 (2005).
- [36] D. A. Steck, *Rubidium 87/85 D Line Data*, available online at <http://steck.us/alkalidata> (revision 2.3.3, 28 May 2024).
- [37] R. Curl, Jr., *Mol. Phys.* **9**, 585 (1965).
- [38] C. V. Rice and D. Raftery, *J. Chem. Phys.* **117**, 5632 (2002).
- [39] D. K. Walter, W. Happer, and T. G. Walker, *Phys. Rev. A* **58**, 3642 (1998).
- [40] M. Repiský, S. Komorovský, V. G. Malkin, O. L. Malkina, M. Kaupp, and K. Ruud, with contributions from R. Bast, U. Ekström, S. Knecht, I. Malkin Ondik, and E. Malkin, ReSpect, relativistic spectroscopy DFT program, version 3.3.0, <http://www.respectprogram.org>.
- [41] J. P. Perdew, M. Ernzerhof, and K. Burke, *J. Chem. Phys.* **105**, 9982 (1996); C. Adamo and V. Barone, *Chem. Phys. Lett.* **298**, 113 (1998); C. Adamo and V. Barone, *J. Chem. Phys.* **110**, 6158 (1999).
- [42] P. Manninen and J. Vaara, *J. Comput. Chem.* **27**, 434 (2006).
- [43] M. Hanni, P. Lantto, M. Repiský, J. Mareš, B. Saam, and J. Vaara, *Phys. Rev. A* **95**, 032509 (2017).
- [44] J. Roukala, J. Zhu, C. Giri, K. Rissanen, P. Lantto, and V.-V. Telkki, *J. Am. Chem. Soc.* **137**, 2464 (2015).
- [45] The small-exponent Gaussian primitives were added to improve the description of the internuclear region of the electron cloud. The exponent values were obtained by dividing the lowest existing exponent by three for each  $l$  value.
- [46] See supplemental material at <http://...> for quantum-chemically calculated spin Hamiltonian parameters, average polarization transfer to  $^{129}\text{Xe}$  with and without Rb hyperfine interaction, examples of polarization transfer

- vs. time in binary collisions at  $B = 1$  mT, Rb nuclear spin polarization in example van der Waals complexes and binary collisions, electron spin polarization level in example binary collisions, construction of the simplified model van der Waals complex, the parameters of the Rabi oscillation analysis of the occupation probabilities in the model van der Waals complex, the relation of the latter to the polarization transfer, transition rates between the states of the model, the effect of the magnetic-field strength on the polarization transfer to  $^{129}\text{Xe}$ , and magnetic field-dependence of the energy levels of the three-spin models.
- [47] T. M. Tierney, N. Holmes, S. Mellor, J. D. López, G. Roberts, R. M. Hill, E. Boto, J. Leggett, V. Shah, M. J. Brookes, R. Bowtell, and G. R. Barnes, *Neuroimage* **199**, 598 (2019).
- [48] B. Driehuys, G. D. Cates, E. Miron, K. Sauer, D. K. Walter, and W. Happer, *Appl. Phys. Lett.* **69**, 1668 (1996).
- [49] N. Ramsey, E. Miron, X. Zeng, and W. Happer, *Chem. Phys. Lett.* **102**, 340 (1983).
- [50] In the perturbed VDW complex depicted in Fig. 3(b), the bond-length oscillation amplitude happens to decrease after each intermediate three-body event. This is not a general feature, and both amplitude increase and decrease occur in the simulated complexes.
- [51] B. Song, Y. Wang, and N. Zhao, *Phys. Rev. A* **104**, 023105 (2021)
- [52] C. Kiehl, D. Wagner, T.-W. Hsu, S. Knappe, C. A. Regal, and T. Thiele, *Phys. Rev. Res.* **5**, L012002 (2003).
- [53] N. D. Bhaskar, W. Happer, M. Larsson, and X. Zeng, *Phys. Rev. Lett.* **50**, 105 (1983).
- [54] M. P. Augustine and K. W. Zilm, *Mol. Phys.* **89**, 737 (1996).
- [55] M. Douglas and N. M. Kroll, *Ann. Phys.* **82**, 89 (1974); B. A. Hess, *Phys. Rev. A* **33**, 3742 (1986).
- [56] F. Neese, *WIREs Comput. Mol. Sci.* **2**, 73 (2012); *Ibid.* **8**, e1327 (2017).
- [57] M. S. Rosen, T. E. Chupp, K. P. Coulter, R. C. Welsh, and S. D. Swanson, *Rev. Sci. Instrum.* **70**, 1546 (1999).
- [58] P. Hilla, M. Tuomela, J. Rantaharju, and J. Vaara, Event trajectories extracted from the MD simulation, spin dynamics simulation code, quantum-chemical input and output files for the NQC tensors, model quantum-chemical input file for the HFC- and  $g$ -tensor data (calculated in Ref. 20), doi: fd-7f2118d0-ab3c-34cb-bacf-27cd5381dc3e